PML AS AN EFFICIENT ABC FOR LOSSY MEDIA

Y. H. Chen and W. C. Chew
Center for Computational Electromagnetics
Department of Electrical and Computer Engineering
University of Illinois
Urbana, IL 61801

Michael L. Oristaglio
Electromagnetics Department
Schlumberger-Doll Research
Old Quarry Road, Ridgefield, CT 06877

Corresponding Author:

W. C. Chew
Center for Computational Electromagnetics
Department of Electrical and Computer Engineering
University of Illinois
Urbana, IL 61801

Abstract

Berenger's perfectly matched layers (PML) has been found very efficient as a material absorbing boundary condition (ABC) for finite-difference time-domain (FDTD) modeling of lossless media. In this paper, we apply the PML ABC to lossy media. The new ABC is shown to work excellently for lossy media too, provided that the appropriate PML profiles are selected. We find that an efficient PML profile is usually related to the medium loss. A general rule is given on the selection of the appropriate PML profiles for media with different losses. A three dimensional (3D) FDTD code based on our formulation has been written to verify our ideas. Excellent agreement is achieved between the FDTD results and the analytical ones for media of different losses. We believe that the PML technique is one of the best ABC's for efficient and precise FDTD modeling.

PML AS AN EFFICIENT ABC FOR LOSSY MEDIA

Y. H. Chen and W. C. Chew
Center for Computational Electromagnetics
Department of Electrical and Computer Engineering
University of Illinois
Urbana, IL 61801

Michael L. Oristaglio
Electromagnetics Department
Schlumberger-Doll Research
Old Quarry Road, Ridgefield, CT 06877

1. Introduction

The method of perfectly matched layers (PML) has been proposed by Berenger [1] for finite-difference time-domain (FDTD) method. The new method aroused enthusiastic response in the electromagnetics community. Many papers [2–9] have been published on the subject, but almost all of them deal with lossless media. For applications such as subsurface geophysical probing, medical imaging, non-destructive testing, etc., the host medium is often conductive. For conductive media, only material absorbing boundary conditions (ABC's) have been used to truncate the simulation region. PML, as a material ABC, is an excellent candidate. PML for lossy media was first studied by Fang and Wu [9]. The main concerns here are whether the medium loss affects the efficiency of the PML ABC, and what PML materials should be chosen for lossy media. In this paper, we show that different PML material profiles are required for media with different degrees of loss. A general rule is given on the choice of the appropriate PML material profiles for lossy media. To verify our formulation, a modified 3D FDTD code has been written based on standard Yee algorithm [10]. We present some dipole waveforms compared against analytical ones for media with different losses. A large three-dimensional (3D), elongated region is chosen for the simulations to maximize ABC reflection effect and to show the efficiency of our PML material profiles. Our results show that our PML ABC works efficiently for both lossless and lossy media. Only ten PML layers are needed to reduce reflection to less than five percent. In what follows, we will first present our PML formulation for lossy media, then analyze the PML material profiles appropriate for lossy media. Numerical results will be given afterwards to support our PML formulation and the selection of the PML material profiles. Finally, we present the conclusions of the paper.

2. PML Formulation for Lossy Media

For a general medium with parameters (ϵ, μ, σ), the modified Maxwell's equations in the frequency domain, as defined by Chew and Weedon [3] assuming $e^{-i\omega t}$, can be written as

$$\nabla_e \times \mathbf{E} = i\omega\mu\mathbf{H}, \tag{1}$$

$$\nabla_h \times \mathbf{H} = -i\omega\epsilon\mathbf{E} + \sigma\mathbf{E}, \tag{2}$$

$$\nabla_h \cdot \epsilon\mathbf{E} = \rho, \tag{3}$$

$$\nabla_e \cdot \mu\mathbf{H} = 0, \tag{4}$$

where $\nabla_e = \hat{x}\frac{1}{e_x}\frac{\partial}{\partial x} + \hat{y}\frac{1}{e_y}\frac{\partial}{\partial y} + \hat{z}\frac{1}{e_z}\frac{\partial}{\partial z}$, $\nabla_h = \hat{x}\frac{1}{h_x}\frac{\partial}{\partial x} + \hat{y}\frac{1}{h_y}\frac{\partial}{\partial y} + \hat{z}\frac{1}{h_z}\frac{\partial}{\partial z}$, with e_ξ, h_ξ, ($\xi = x, y$,or z) being the coordinate-stretching variables for the x, y, z coordinates for ∇_e and ∇_h. As we shall see later, the coordinate-stretching variables are actually something related to the properties of the PML materials. Thus, we also call them as PML material profiles. As shown in the paper by Chew and Weedon [3], the coordinate-stretching variables satisfying the following conditions will achieve a perfectly matched boundary interface perpendicular to the z axis if the medium parameters, ϵ and μ, remain the same across the interface,

$$e_{1x} = e_{2x} = h_{1x} = h_{2x}, \tag{5}$$

$$e_{1y} = e_{2y} = h_{1y} = h_{2y}, \tag{6}$$

$$e_{1z}h_{2z} = e_{2z}h_{1z}, \tag{7}$$

where the subscripts 1 and 2 denote the region of interest and the PML region respectively.

In the simulation region, we want to solve the actual Maxwell's equations instead of the modified ones. Thus, we choose the unit value for all the coordinate-stretching variables in region 1, i.e.

$$(e_{1x}, e_{1y}, e_{1z}, h_{1x}, h_{1y}, h_{1z}) = (1, 1, 1, 1, 1, 1). \tag{8}$$

From Equations (5–8), the coordinate-stretching variables in the region 2, or the PML region, can only be

$$(e_{2x}, e_{2y}, e_{2z}, h_{2x}, h_{2y}, h_{2z}) = (1, 1, s(z), 1, 1, s(z)), \tag{9}$$

where $s(z)$ can be selected arbitrarily. However, in order to absorb the waves in the PML region, the variable $s(z)$, or the PML material profile in the z direction, has to be chosen carefully. We choose $s(z)$ to be

$$s(z) = \frac{\beta(z)}{\omega_c \epsilon} + i\frac{\alpha(z)}{\omega \epsilon}, \tag{10}$$

where $\beta(z)$ and $\alpha(z)$ are functions of z, and ω_c is the center frequency of the source. Similar PML material profiles can be selected for other boundary interfaces which are perpendicular to the x and y axes. After substituting the above PML material profiles into Equations (1) and (2), we obtain

$$\frac{\beta(\xi)}{\omega_c \epsilon}\frac{\partial \mathbf{H}_{s\xi}}{\partial t} + \frac{\alpha(\xi)}{\epsilon}\mathbf{H}_{s\xi} = -\frac{1}{\mu}\frac{\partial}{\partial \xi}\hat{\xi} \times \mathbf{E}, \tag{11}$$

$$\frac{\beta(\xi)}{\omega_c \epsilon}\frac{\partial \mathbf{E}_{s\xi}}{\partial t} + \left(\frac{\beta(\xi)}{\omega_c \epsilon}\frac{\sigma}{\epsilon} + \frac{\alpha(\xi)}{\epsilon}\right)\mathbf{E}_{s\xi} + \frac{\alpha(\xi)}{\epsilon}\frac{\sigma}{\epsilon}\int_{-\infty}^{t}\mathbf{E}_{s\xi}dt = \frac{1}{\epsilon}\frac{\partial}{\partial \xi}\hat{\xi} \times \mathbf{H}, \tag{12}$$

where the vectors $\mathbf{H}_{s\xi}$ and $\mathbf{E}_{s\xi}$ are the transverse components to $\hat{\xi}$ with $\xi = x, y$, or z. The total electromagnetic fields are given by $\mathbf{E} = \mathbf{E}_{sx} + \mathbf{E}_{sy} + \mathbf{E}_{sz}$, and

$\mathbf{H} = \mathbf{H}_{sx} + \mathbf{H}_{sy} + \mathbf{H}_{sz}$. Equations (11) and (12), with $\xi = x, y$, or z, describe a 3D wave propagation in a conductive medium with PML absorbing materials at the boundaries. Standard Yee scheme can be used to solve for the electromagnetic fields.

3. PML Material Profiles for Lossy Media

Does the medium loss affect the efficiency of the PML ABC? What PML material profiles should be chosen for conductive media? Let us consider a PML region illustrated in Figure 1, where we assume that the artificial boundary is perpendicular to the z axis and the incident waves are in the yz plane. The z component of the wave propagation constant in the PML region can be derived as

$$k_z(z) = \omega\sqrt{\epsilon\mu}\left(1 + i\frac{\sigma}{\omega\epsilon}\right)^{\frac{1}{2}}\left[\frac{\beta(z)}{\omega_c\epsilon} + i\frac{\alpha(z)}{\omega\epsilon}\right]\cos\theta. \tag{13}$$

If the medium is lossless, Equation (13) becomes

$$k_z(z) = \omega\sqrt{\epsilon\mu}\left[\frac{\beta(z)}{\omega_c\epsilon} + i\frac{\alpha(z)}{\omega\epsilon}\right]\cos\theta. \tag{14}$$

In principle, the PML ABC works because we can control the value of k_z while maintaining same k_x and k_y across the PML layers. The change of k_z is achieved by choosing appropriate $\alpha(z)$ and $\beta(z)$. Although the PML layers theoretically match each other perfectly regardless of what functions $\alpha(z)$ and $\beta(z)$ are, the two functions have to be chosen such that they change gradually to avoid significant numerical reflections as the waves travel and decay through the PML region. As we can see from Equation (14) for lossless media, the real part and the imaginary part of k_z can be easily changed by adjusting $\alpha(z)$ and $\beta(z)$ respectively. The function $\alpha(z)$ makes propagating waves decay along the z axis, and the function $\beta(z)$ causes evanescent waves to attenuate faster in the same direction if they exist. Here, we assume that both $\alpha(z)$ and $\beta(z)$ are non-negative functions of z. Note that for evanescent waves, $\cos\theta$ is imaginary.

For conductive media, however, the z component of the propagation constant k_z not only depends on the functions $\alpha(z)$ and $\beta(z)$, but also depends on the medium loss $\frac{\sigma}{\omega\epsilon}$. It is not possible to design any single PML material profile which can absorb waves for a conductive medium of arbitrary loss. We choose to treat the conductive media separately depending on their loss. For a low loss medium ($\frac{\sigma}{\omega\epsilon} \ll 1$), a handy way is to just treat it as a lossless case. For a high loss medium ($\frac{\sigma}{\omega\epsilon} \gg 1$), Equation (13) becomes

$$k_z(z) = \sqrt{\frac{\omega\mu\sigma}{2}}\left[f_1(z) + i f_2(z)\right]\cos\theta, \tag{15}$$

where

$$f_1(z) = \frac{\beta(z)}{\omega_c\epsilon} - \frac{\alpha(z)}{\omega\epsilon}, \tag{16}$$

$$f_2(z) = \frac{\beta(z)}{\omega_c\epsilon} + \frac{\alpha(z)}{\omega\epsilon}. \tag{17}$$

In this case, the attenuation of the propagating waves is determined by $f_2(z)$, and the decay of the attenuating waves (including the evanescent waves) is controlled by $f_1(z)$. We choose $\beta(z)$ to be much larger than $\alpha(z)$ to make the real part of $k_z(z)$ non-negative. As the medium conductivity increases, however, the incident waves at the boundaries consist predominantly of low frequency components. The second term in $f_1(z)$ can still grow to cause the real part of $k_z(z)$ to be negative or zero. To overcome this, we choose function $\beta(z)$ to be approximately proportional to the host medium conductivity σ. For media with $\frac{\sigma}{\omega\epsilon} \approx 1$, $k_z(z)$ can be approximated as

$$k_z(z) \approx \omega\sqrt{\epsilon\mu}\left[\left(1.10\frac{\beta(z)}{\omega_c\epsilon} - 0.46\frac{\alpha(z)}{\omega\epsilon}\right) + i\left(0.46\frac{\beta(z)}{\omega_c\epsilon} + 1.10\frac{\alpha(z)}{\omega\epsilon}\right)\right]. \tag{18}$$

Equation (18) is very similar to Equation (15) when the function $\beta(z)$ is dominant over $\alpha(z)$. We treat this case in the same way as what we did for high loss media.

4. Numerical Results

Based on the above formulation, a 3D FDTD code was written and parallelized on an SGI Power Challenge machine to simulate the fields of an electric dipole source in lossless and lossy media. As shown in Figure 2, an elongated region is specifically chosen to maximize the reflection from the side boundaries. The size of the simulation region chosen is 0.75 m $\times$ 0.75 m $\times$ 3. m in the x, y, and z directions correspondingly. We discretize the region using a uniform grid size of 0.025 m. The source is located at $(x, y, z) = (0.4, 0.4, 0.2)$ m and the receivers are located at $x = y = 0.35$ m, $z = (0.25, 0.5, 0.75, 1., 1.25, 1.5, 1.75, 2., 2.25, 2.5, 2.75, 3.)$ m. The source used is the first derivative of the Blackman-Harris window function [11] pointing in the z direction with a center frequency of 600 MHz. The Blackman-Harris window function is given by

$$f(t) = \begin{cases} \sum_{n=0}^{3} a_n \cos(2n\pi t/T), & \text{if } 0 < t < T, \\ 0, & \text{otherwise,} \end{cases} \tag{19}$$

where T is the duration of the source function. The coefficients used are

$$a_0 = 0.35322222, \quad a_1 = -0.488, \quad a_2 = 0.145, \quad a_3 = -0.010222222. \tag{20}$$

The source duration T is given by

$$T = \frac{1.55}{f_c}, \tag{21}$$

where f_c is the center frequency of the source. For f_c =600 MHz, the first derivative of the Blackman-Harris window function is shown in Figure 3.

Figures 4 and 5 are the simulation results of H_x compared against the analytical results given by Song and Chen [12], and Chew [13] for lossy media with different conductivities. The solid lines are the results of our FDTD code recorded at different locations in the z direction and the dashed lines are calculated analytically. Each line has been normalized to give a maximum amplitude of unity. In Figure 4 different numbers of PML layers are used outside the FDTD simulation region to test the efficiency of our PML ABC. The medium has a conductivity of 0.01 S/m. The numbers of PML layers used for Figures 4(a)–(d) are ten, five, three, and zero correspondingly. As we can see from the results, ten PML layers are good enough to absorb most of the incident waves at the boundaries. The slight discrepancies between the numerical and the analytical results in Figure 4(a) are caused by grid dispersion and can be reduced by decreasing the grid size. A broad range of medium conductivity is used to test the effectiveness of our PML formulation for lossy media. As shown in Figures 5(a)–(e), excellent agreement between our numerical results and the analytical results is achieved. The waveforms become smoother as the waves propagate away from the source due to the diffusion phenomenon. For the above examples, a single model is used for simplicity. The code has also been tested with models of different sizes and with sources of different center frequencies. For all the test cases performed, very good results have been achieved.

5. Conclusions

A new formulation has been given to apply the newly-proposed PML concept to lossy media for FDTD simulations ranging from the wave equation to the diffusion equation regimes. The selection of a PML material profile turns out to be the key for the PML ABC to work effectively. A PML material profile working for a lossless medium usually does not work for a lossy medium. In fact, any PML material profile will not be effective for a general host medium if the medium loss is not taken into account. A 3D FDTD code based on this formulation has been written to test our ideas in Cartesian coordinates. Excellent agreement was achieved for all the test cases between our numerical results and the analytical results. The code works for host media of arbitrary loss. Our PML material profile turns out to be very efficient. Only ten PML layers are needed to reduce reflections to less than 5 percent. We believe that the PML technique is one of the most important ABC's for efficient and precise FDTD modeling.

References

[1] J. P. Berenger, "A Perfectly Matched Layer for the Absorption of Electromagnetic Waves," *J. Computat. Phys.*, vol. 114, no. 2, pp. 185–200, Oct. 1994.

[2] D. S. Katz, E. T. Thiele, and A. Taflove, "Validation and Extension to Three Dimensions of the Berenger PML Absorbing Boundary Condition for FD-TD Meshes," *IEEE Microwave and Guided Wave Lett.*, vol. 4, no. 8, pp. 268–270, Aug. 1994.

[3] W. C. Chew and W. H. Weedon, "A 3D Perfectly Matched Medium from Modified Maxwell's Equations with Stretched Coordinates," *Microwave and Opt. Tech. Lett.*, vol. 7, no. 13, pp. 599–604, Sept. 1994.

[4] E. A. Navarro, C. Wu, P. Y. Chung, and J. Litva, "Application of PML Superabsorbing Boundary Condition to Non-Orthogonal FDTD Method," *Electron. Lett.*, vol. 30, no. 20, pp. 1654–1656, Sept. 1994.

[5] M. Gribbons, S. K. Lee, and A. C. Cangellaris, "Modification of Berenger's Perfectly Matched Layer for the Absorption of Electromagnetic Waves in Layered Media," *Proc. 11th Ann. Rev. of Progress in ACES*, Monterey, CA, Mar. 20–25, 1995, pp. 498–503.

[6] R. Mittra and Ü. Pekel, "A New Look at the Perfectly Matched Layer (PML) Concept for the Reflectionless Absorption of Electromagnetic Waves," *IEEE Microwave and Guided Wave Lett.*, vol. 5, no. 3, pp. 84–86, Mar. 1995.

[7] W. V. Andrew, C. A. Balanis, and P. A. Tirkas, "A Comparison of the Berenger Perfectly Matched Layer and the Lindman Higher-Order ABC's for the FDTD Method," *IEEE Microwave and Guided Wave Lett.*, vol. 5, no. 6, pp. 192–194, Jun. 1995.

[8] Z. S. Sacks, D. M. Kingsland, R. Lee, and J. F. Lee, "A Perfectly Matched Anisotropic Absorber for Use as an Absorbing Boundary Condition," *IEEE Trans. Ant. Propagat.*, vol. 43, no. 12, pp. 1460–1463, Dec. 1995.

[9] J. Fang and Z. Wu, "Generalized Perfectly Matched Layer - An Extension of

Berenger's Perfectly Matched Layer Boundary Condition," *IEEE Microwave and Guided Wave Lett.*, vol. 5, no. 12, pp. 451–453, Dec. 1995.

[10] K. S. Yee, "Numerical Solution of Initial Boundary Value Problems Involving Maxwell's Equations in Isotropic Media," *IEEE Trans. Ant. Propagat.*, vol. AP-14, pp. 302–307, 1966.

[11] F. J. Harris, "On the Use of Windows for Harmonic Analysis with the Discrete Fourier Transform," *Proc. IEEE*, vol. 66, no. 1, pp. 51–83, 1978.

[12] J. Song and K. M. Chen, "Propagation of EM Pulses Excited by an Electric Dipole in a Conducting Medium," *IEEE Trans. Ant. Propagat.*, vol. 41, no. 10, pp. 1414–1421, Oct. 1993.

[13] W. C. Chew, *Waves and Fields in Inhomogeneous Media,* Van Nostrand, New York, 1990.

Figure Captions

Figure 1. Outgoing waves illuminating a PML boundary.

Figure 2. Elongated simulation region designed to maximize the side reflections.

Figure 3. The first derivative of the Blackman-Harris window function used as the incident field.

Figure 4. Different numbers of PML layers are used outside the FDTD simulation region to observe the efficiency of the PML ABC for lossy media. The solid lines are the waveforms of FDTD results, and the dashed lines are the analytical solutions. The medium conductivity $\sigma = 0.01$ S/m. (a) Ten PML layers are used. (b) Five PML layers are used. (c) Only three PML layers are used. (d) No PML layers are used.

Figure 5. Waveform comparison of the FDTD results (solid lines) and the analytical solutions (dashed lines) for a dipole source in lossless and lossy media. (a) Lossless medium, (b) $\sigma = 0.02$ S/m, (c) $\sigma = 0.04$ S/m, (d) $\sigma = 0.16$ S/m, (e) $\sigma = 0.80$ S/m.

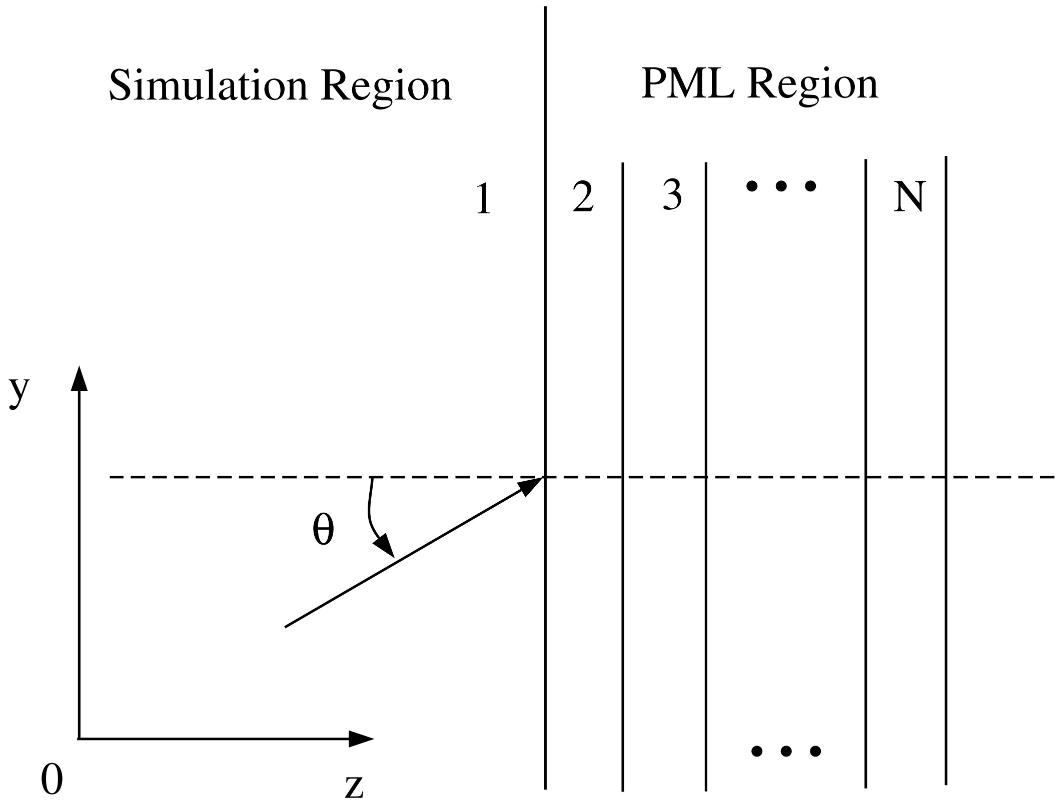

Figure 1. Outgoing waves illuminating a PML boundary.

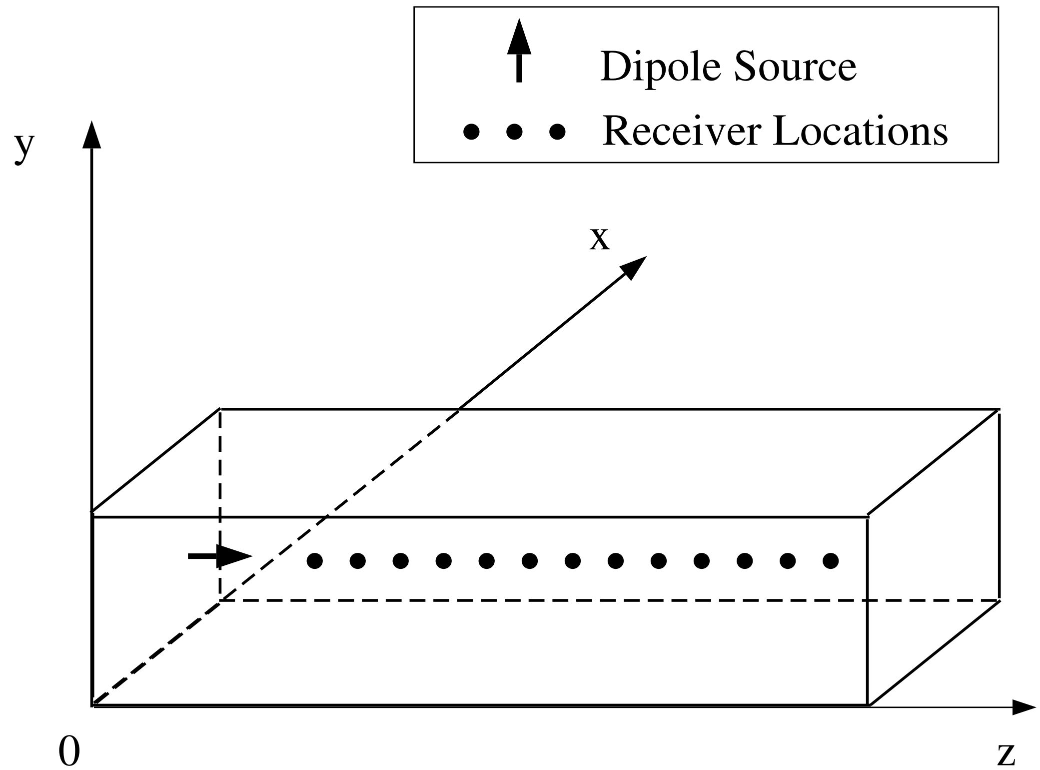

Figure 2. Elongated simulation region designed to maximize the side reflections.

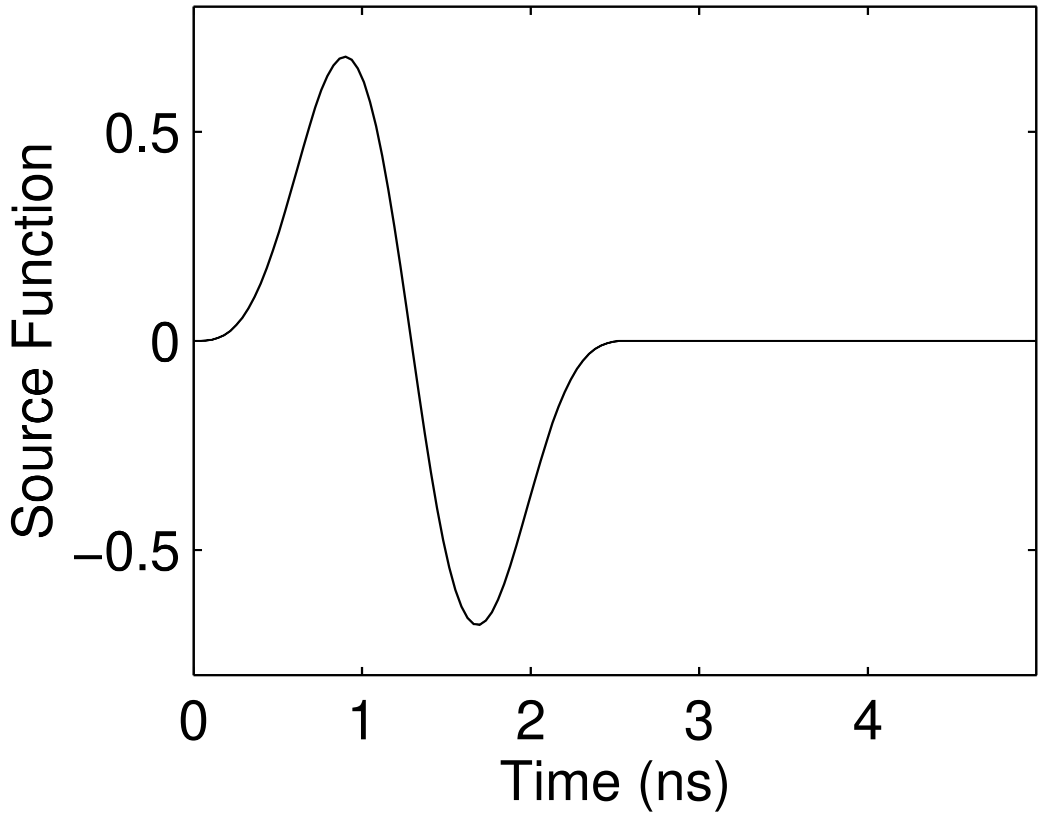

Figure 3. The first derivative of the Blackman-Harris window function used as the incident field.

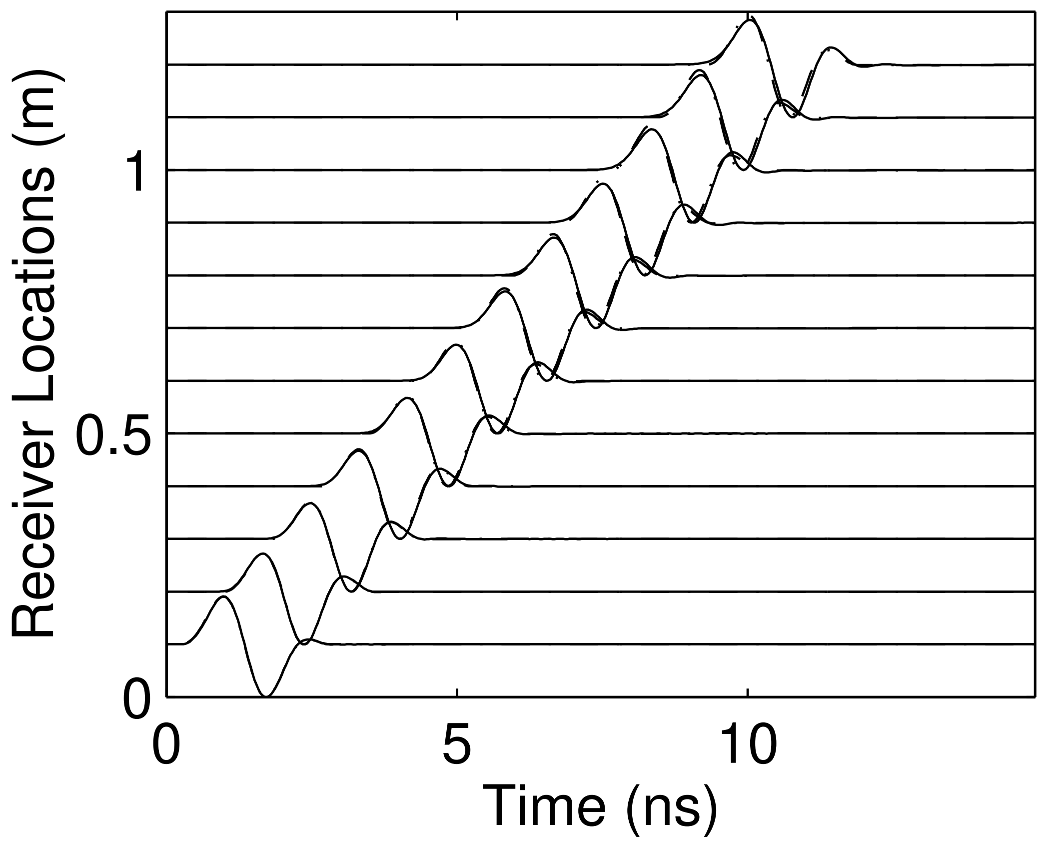

Figure 4(a). Different numbers of PML layers are used outside the FDTD simulation region to observe the efficiency of the PML ABC for lossy media. The solid lines are the waveforms of FDTD results, and the dashed lines are the analytical solutions. The medium conductivity $\sigma = 0.01$ S/m. The number of PML layers used is 10.

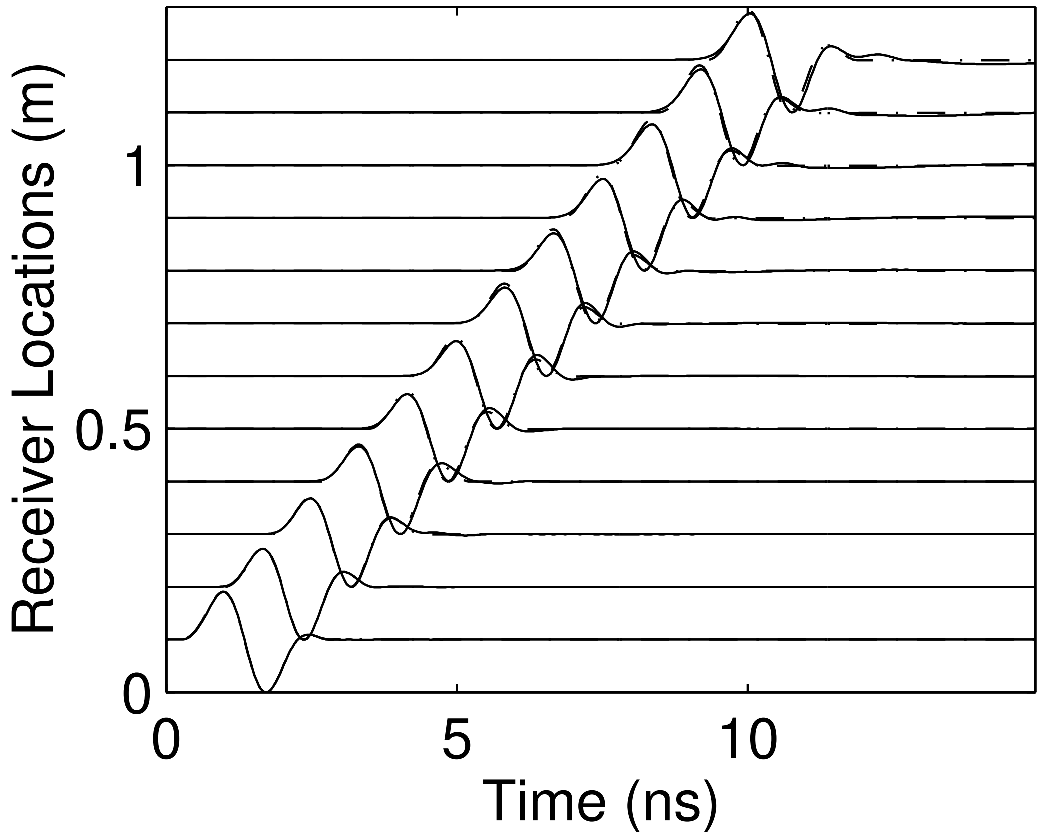

Figure 4(b). Different numbers of PML layers are used outside the FDTD simulation region to observe the efficiency of the PML ABC for lossy media. The solid lines are the waveforms of FDTD results, and the dashed lines are the analytical solutions. The medium conductivity $\sigma = 0.01$ S/m. Only 5 PML layers are used.

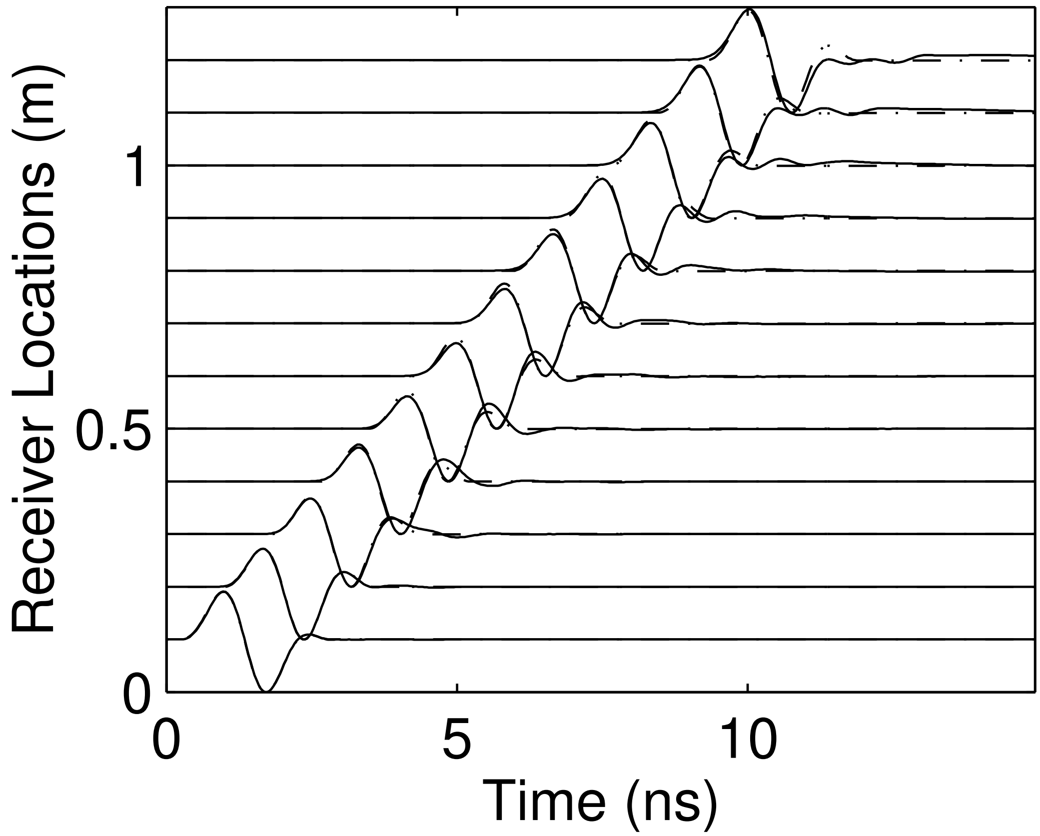

Figure 4(c). Different numbers of PML layers are used outside the FDTD simulation region to observe the efficiency of the PML ABC for lossy media. The solid lines are the waveforms of FDTD results, and the dashed lines are the analytical solutions. The medium conductivity $\sigma = 0.01$ S/m. Only 3 PML layers are used.

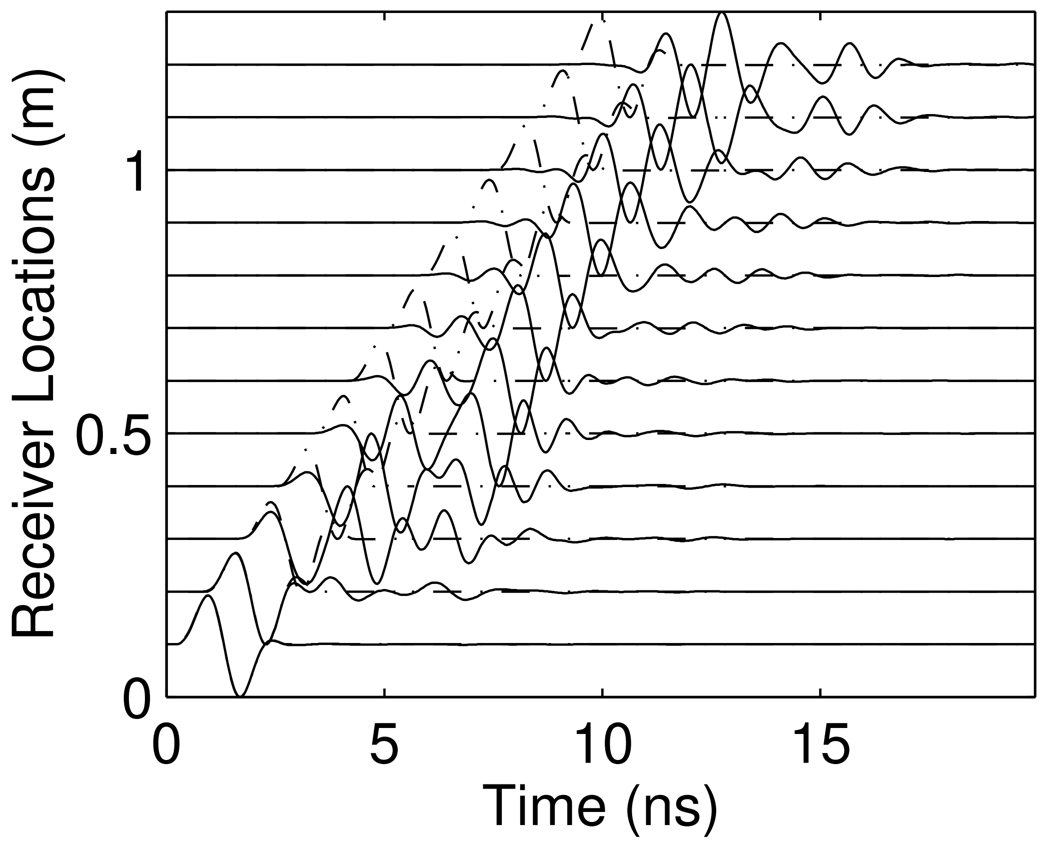

Figure 4(d). Different numbers of PML layers are used outside the FDTD simulation region to observe the efficiency of the PML ABC for lossy media. The solid lines are the waveforms of FDTD results, and the dashed lines are the analytical solutions. The medium conductivity $\sigma = 0.01$ S/m. No ABC is used.

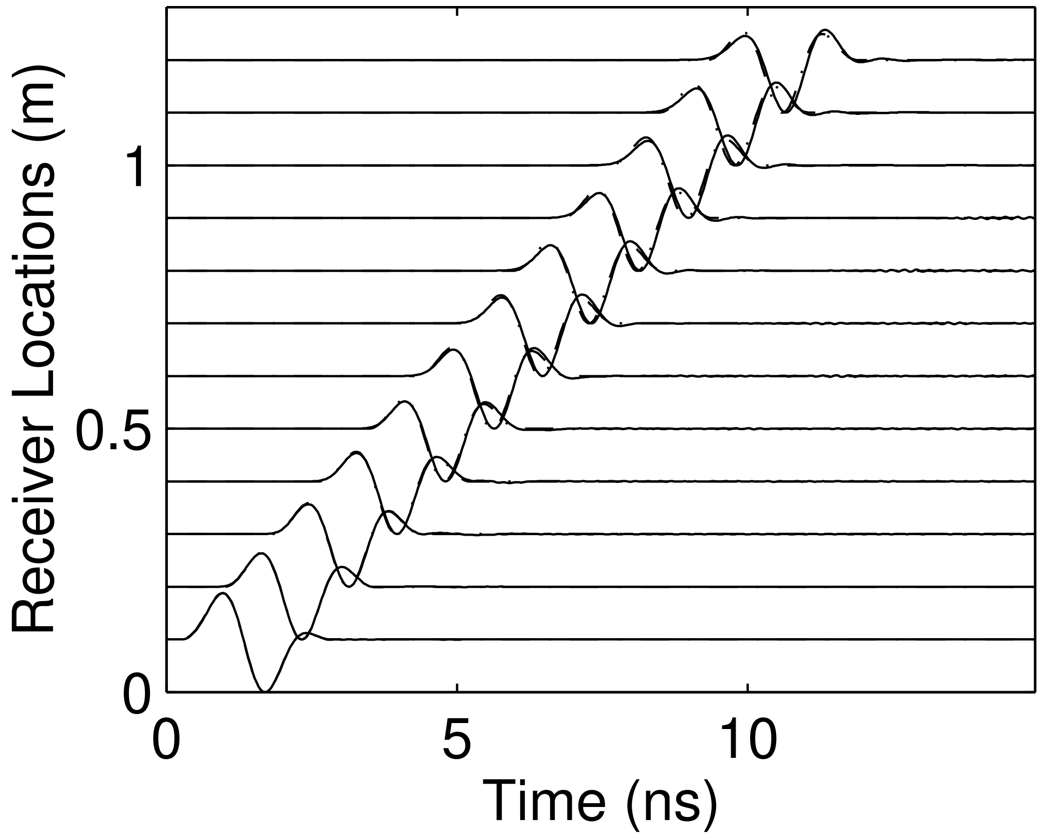

Figure 5(a). Waveform comparison of the FDTD results (solid lines) and the analytical solutions (dashed lines) for a dipole source in a lossless medium.

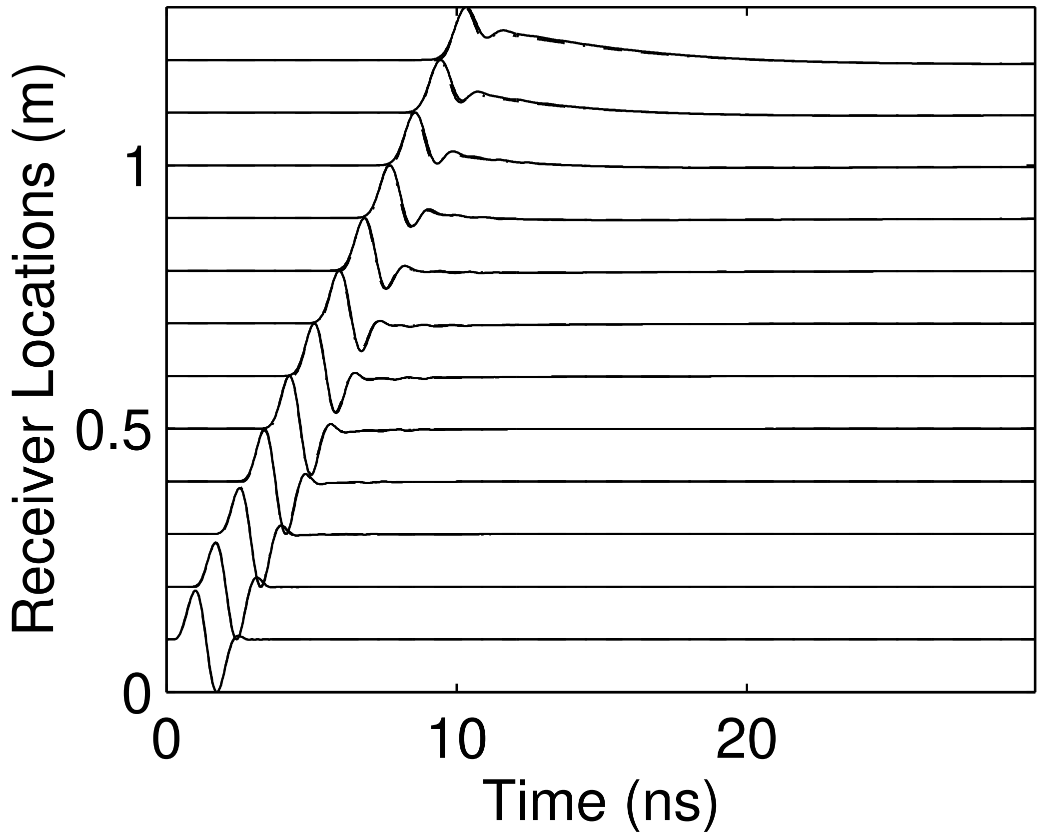

Figure 5(b). Waveform comparison of the FDTD results (solid lines) and the analytical solutions (dashed lines) for a dipole source in a lossy medium ($\sigma = 0.02$ S/m).

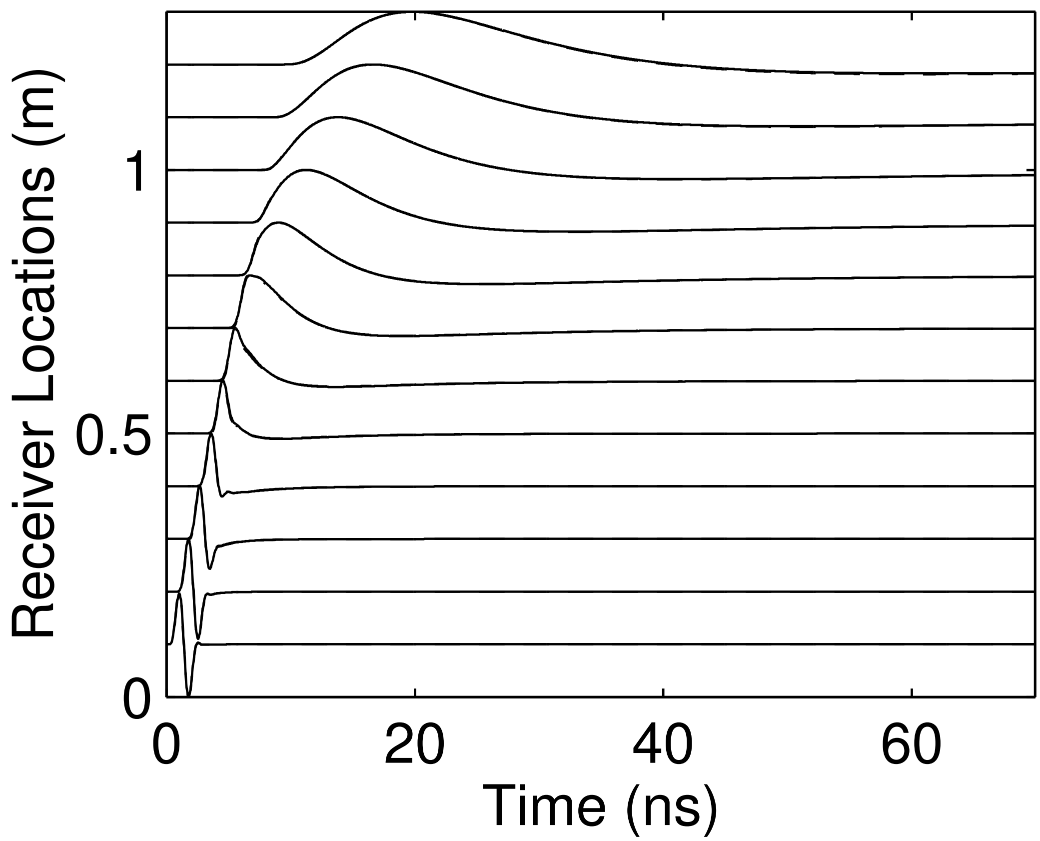

Figure 5(c). Waveform comparison of the FDTD results (solid lines) and the analytical solutions (dashed lines) for a dipole source in a lossy medium ($\sigma = 0.04$ S/m).

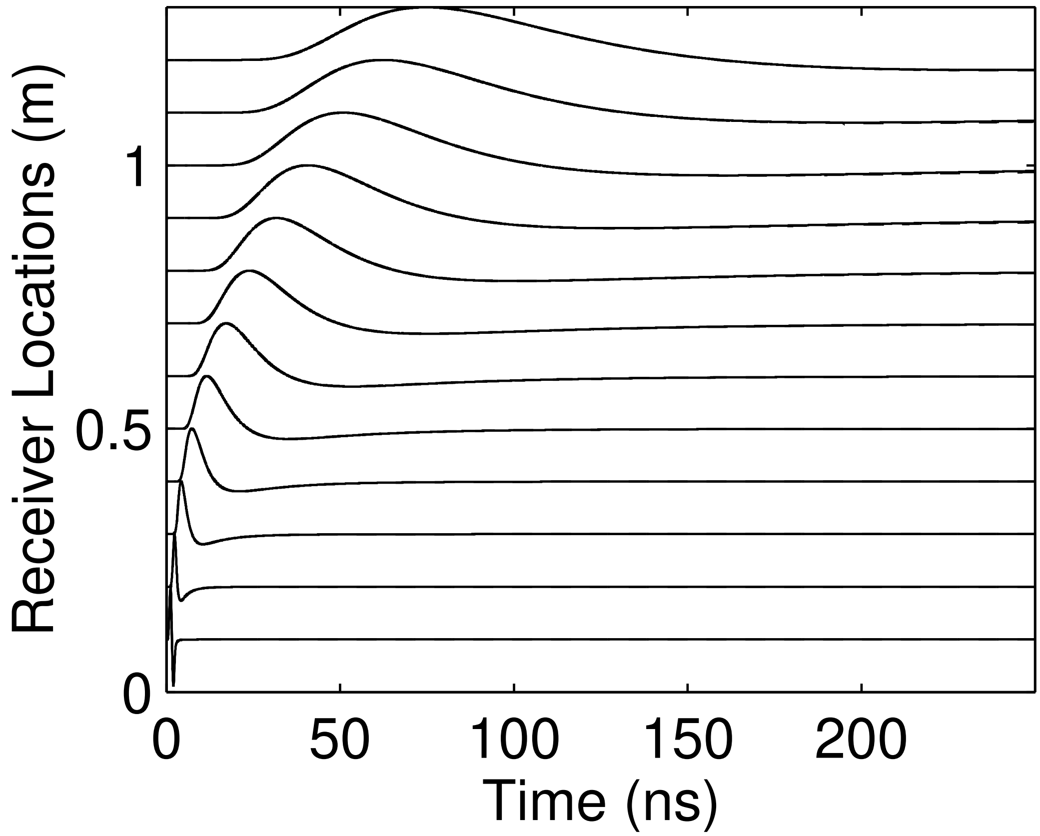

Figure 5(d). Waveform comparison of the FDTD results (solid lines) and the analytical solutions (dashed lines) for a dipole source in a lossy medium ($\sigma = 0.16$ S/m).

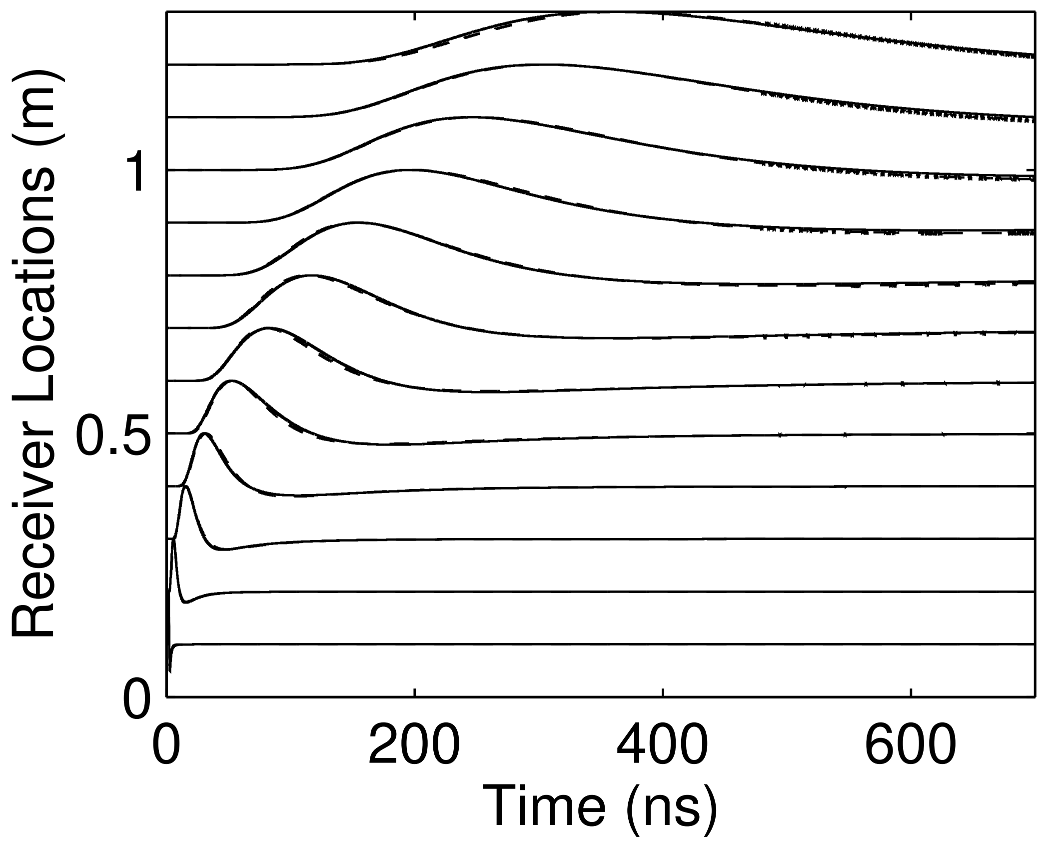

Figure 5(e). Waveform comparison of the FDTD results (solid lines) and the analytical solutions (dashed lines) for a dipole source in a lossy medium ($\sigma = 0.80$ S/m).